 ©2013 Kvantovaya Elektronika and Turpion Ltd

PACS numbers: 42.65.Re; 42.65.Jx; 52.50.Jm
DOI: 10.1070/QE2013v043n04ABEH015112

Experimental study of filamentation of high-power ultrashort laser pulses with initial angular divergence in air

Yu.E. Geints, A.A. Zemlyanov, A.M. Kabanov, G.G. Matvienko, A.N. Stepanov

Abstract. **Experimental study of the nonlinear propagation of near-IR gigawatt femtosecond laser pulses in air in the self-focusing and filamentation regimes have been performed in open air and in laboratory. The influence of the initial geometric divergence (both positive and negative) of the laser beam with an irregular intensity profile on the transverse light energy distribution at the end of the path is studied. It is shown experimentally that the displacement of the filamentation region due to geometric focusing or defocusing, makes it possible to control the number and spatial location of light energy density peaks in the receiving plane. The conditions under which a light filament can be reconstructed after the beam transmission through a linear focal waist are determined. A semi-empirical threshold relation is obtained for the beam focusing force and the beam power, when light beam undergoes filamentation behind the geometric focus of the optical system.**

Keywords: *filamentation of femtosecond laser beam, angular divergence, multiple filaments.*

1. Introduction

The problem of laser energy transport through an atmosphere and its delivery to a detector with minimum loss is of prime importance for atmospheric optics. This problem implies primarily a complex of measures on keeping geometric light-beam sizes within a specified aperture at the end of the beam path. In most cases this result is obtained by means of initial geometric focusing of the beam to the detector. At the same time, a number of applied problems call not only for conservation of a specified beam cross section area but also for formation of spatially localised regions of higher intensity (energy density) in the target, i.e., extreme concentration of laser energy in the beam. Currently, under real atmospheric conditions this problem can be solved using laser beam self-focusing and filamentation.

The physical nature of self-focusing is cubic optical nonlinearity of the medium (Kerr nonlinearity), which causes a self-induced increase in the refractive index of the medium; this increase is proportional to the light intensity. When a light pulse with a sufficiently high (exceeding some threshold value) power propagates in a medium, it undergoes increasing compression in all transverse directions. This process is actively hindered by the diffraction of light and some physical mechanisms, among which multiphoton absorption and plasma formation dominate in gases and condensed media.

Nonlinear absorption in the medium leads to energy loss in the beam channel, as a result of which the light intensity ceases to grow. In addition, the plasma generated hinders Kerr self-focusing due to the decrease in the nonlinear refractive index. The dynamic balance of focusing and defocusing 'forces' results in the following: beginning with a certain point in the path, high-intensity regions, localised in space and in time (nonlinear foci), are formed in the light pulse. These foci, having a quasi-constant intensity (up to 10^{14} W cm^{-2}) and a weakly changing transverse size (generally, about 100 μm), may exist on a rather long fragment of the path (up to several beam diffraction lengths). When propagating along with the pulse, nonlinear foci leave traces on the path (referred to as filaments), which look like luminous thin threads due to the fluorescence of plasma-excited nitrogen molecules. Furthermore, due to energy loss on plasma formation and beam divergence, the force balance that gives rise to filamentation becomes violated and filamentation ceases. The modern state of the problem of self-focusing and filamentation of ultrashort laser pulses (USLPs) was comprehensively analysed in reviews [1–3] and monographs [4, 5].

As was noted above, the beam self-focusing is a threshold effect. The threshold (critical) self-focusing power P_c for atmospheric air in the mid-IR range is several gigawatts. Obviously, to overcome the self-focusing threshold, the radiation should have an initial power $P_0 > P_c$. This condition is satisfied, for example, for femtosecond pulses of a Ti:sapphire laser with the centre wavelength $\lambda_0 \approx 800$ nm and energy of several tens of millijoules.

Formally speaking, Kerr nonlinearity of a medium forms a kind of an aberration lens, which not only provides geometric focusing but also forms a new nonlinear focus, which is always located on the path at a distance closer than the linear focus of the optical system. Therefore, to solve the problem of the energy transfer of femtosecond radiation with a high power density along an atmospheric path, one must know how to control the position of this nonlinear focus.

To date, several methods for controlling the length at which filaments are formed in a high-power light beam propagating in air have been developed and experimentally implemented. They include variation in the initial angular beam divergence [6, 7], modulation of the initial amplitude distribution (diaphragm, introduction of artificial aberrations) [8–10]

Yu.E. Geints, A.A. Zemlyanov, A.M. Kabanov, G.G. Matvienko
V.E. Zuev Institute of Atmospheric Optics, Siberian Branch, Russian Academy of Sciences, pl. Akad. Zueva 1, 634021 Tomsk, Russia;
e-mail: ygeints@ao.ru;
A.N. Stepanov Institute of Applied Physics, Russian Academy of Sciences, ul. Ul'yanova 46, 603950 Nizhnii Novgorod, Russia
e-mail: step@ufp.appl.sci-nnov.ru

Received 24 December 2012; revision received 18 January 2013
Kvantovaya Elektronika **43** (4) 350–355 (2013)
Translated by Yu.P. Sin'kov

or light field phase (chirping) [11, 12], and variation in the initial beam size (telescoping) [13, 14]. Each of these techniques has advantages and drawbacks, which are mainly related to difficulties in their technical realisation; the latter determine the efficiency of specific technique [2, 15].

Traditionally, geometric beam focusing is the most efficient way of controlling the position of the filamentation region on short and moderately long (up to a kilometre) optical paths [6]. Here, one must take into account that focusing gives rise to some specific features in the beam filamentation. The most significant one is the decrease in the total length of the region where filaments exist behind the beam focal waist. It was established that manifestation of this effect depends on both the initial laser pulse power and the beam focusing tightness [16], as well as on the filamentation regime (single or multiple) [3, 17]. Indeed, a high beam divergence after the geometric focus may suppress filamentation. In the region of the linear focal waist, the beam-profile-averaged diffraction 'forces' [18] are strongest; therefore, if the beam focusing is sufficiently tight, the laser pulse power may be insufficient for maintaining or resuming filamentation. In this context, an important problem is to establish how tight should be the laser beam focusing, below (above) which filamentation exist (is absent) behind the beam focal plane.

In this paper, we report the results of studying the self-focusing and filamentation of a high-power femtosecond laser beam, characterised by initial geometric focusing (or defocusing), in air. These investigations were based on the results of natural atmospheric and laboratory experiments, performed by us using the femtosecond laser system at the Institute of Applied Physics, Russian Academy of Sciences (Nizhnii Novgorod) in the 2011–2012s. In contrast to most such studies, the high-power laser beam in the case under consideration had initially a non-Gaussian, sharply nonuniform (over the beam cross section) spatial intensity profile; this circumstance manifested itself in the self-focusing properties. Nevertheless, the results presented below showed that even under these conditions there is a real possibility of controlling the spatial shape of the laser beam cross section in the reception zone using focusing or defocusing of the initial beam. In addition, laboratory study and theoretical analysis revealed the conditions under which a light filament can be recovered after the beam is transmitted through the linear focus of the system.

2. Experiments and discussion of results

The experiments were performed on a terawatt femtosecond laser system of the Institute of Applied Physics (Nizhnii Novgorod) [19]. The master oscillator was a passively mode-locked Ti : sapphire laser based on the Kerr mechanism. The femtosecond laser was pumped by spatially single-mode (TEM_{00q} mode) second harmonic of a cw solid-state Nd : YAG laser with $\lambda_0 = 532$ nm. The diameter d of the Ti:sapphire crystal in the final amplifier was 15 mm. We applied a diffraction grating 200 × 100 mm in size with the following characteristics: 1600 lines mm^{-1}, reflectance 90%, and radiation resistance (for a pulse duration of 1 ns) of 1 J cm^{-2}. The experiments were performed using the main harmonic of the Ti : sapphire laser ($\lambda_0 = 800$ nm) in the regime of self-focusing and filamentation in air. The maximum energy E_0 of a single laser pulse exceeded 100 mJ. The characteristic FWHM of the laser pulse, t_p, found by calibrating the autocorrelation function, was 66 fs with a 10^3 time contrast at 1 ps and a pulse repetition rate of 10 Hz. Single-shot regime was also used. The laser pulse energy was varied using a polarisation attenuator and monitored by a photodiode calibrated with a pyroelectric sensor (Molectron J25LP).

The pulse energy in the atmospheric experiments with a telescoped beam did not exceed 40 mJ (this limitation is related to the damage threshold of the defocusing mirror of the telescope). A system composed of mirrors (focusing and defocusing) was applied to form a convergent or divergent beam on an atmospheric path of length $L = 85$ m; this was done by, respectively, reducing or increasing the telescope base. The maximum beam size at half maximum at the telescope output was ~8 mm. In the laboratory measurements the maximum optical path length after the focusing system was 4.39 m, and focusing was performed by a spherical mirror with a focal length of 125 cm.

We used a 12-bit CCD camera (Hamamatsu c8484-05G) and a Canon EOS 500D camera in the experiments to record the light energy distribution over the laser beam cross section on a white screen located at a distance of 85 m from laser radiation source. The longitudinal energy profile in the filament in the zone of the geometric mirror focus was recorded by detecting the nitrogen fluorescence signal using a 12-bit CCD camera (PCO, PixelFly VGA) perpendicularly to the laser beam axis.

2.1. Experiments in open air

Examples of light energy spatial distribution over the laser beam cross section at the end of the atmospheric path are shown in Fig. 1. The bright spots in the photographs correspond to higher laser energy densities and are projections of filaments onto a recording screen. It is noteworthy that the character of the spatial distribution of these bright spots over the beam cross section and their size depend on the telescope focal length.

For example, the initially collimated beam at the end of the path (Fig. 1a) is transformed into a single low-divergent light channel, located near the telescope optical axis and surrounded by weak secondary channels. As was mentioned above, these channels are in essence traces of the filaments that were formed at the beginning of the optical path and decayed at the end of the path. The main channel may be a filament survived as a result of competition.

The focused beam ($f > 0$, Figs 1b–d) demonstrates quite a different pattern of the light energy distribution during filamentation. As follows from the self-focusing theory [20], any external focusing of radiation shifts the filamentation onset to the beginning of the path, which, in turn, decreases the total length of the region where filaments exist. As a result, the beam filamentation stopped before the beam profile was recorded (at the end of the path), as is evidenced by the strong diffusion of the projection of the 'main' filament even at the softest focusing used (Fig. 1b). A further decrease in the telescope focal length only enhances this effect: at $f < 25$ m the laser beam transverse size exceeded the size of the photodetector recording region.

In the opposite case, where the beam was initially defocused ($f < 0$), bright spots of approximately equal luminescence intensity are observed in the top left corner of the image (Figs 1e–g). The small size of these spots (compare with Fig. 1a) and their pronounced spatial localisation indicate their relationship with the filaments formed on the path. It is obvious that, due to the initial defocusing of the laser beam, it

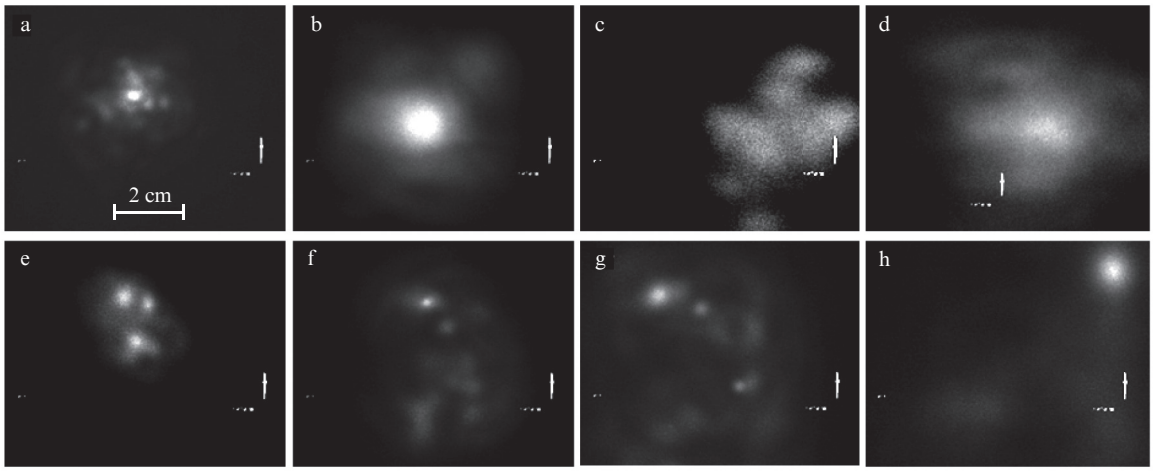

Figure 1. Transverse profiles of the energy density of femtosecond laser radiation with E_0 = 9.6 mJ at the end of atmospheric path (85 m) under different focusing conditions: (a) collimated beam; (b–d) focusing with focal lengths f = (b) +75, (c) +36, and (d) +25 m; and (e–h) defocusing with f = (e) –75, (f) –36, (g) –25, and (h) –12.5 m.

undergoes filamentation at a point much closer to the end of the path than in the case of a collimated beam. This fact explains the larger number of light spots recorded by the detector. With an increase in the degree of beam defocusing (i.e., with a decrease in $|f|$), the spatial spread of filaments over the beam cross section also increases, and their number decreases (Fig. 1h).

Figure 2 shows the results of processing the spatial profiles of the beam intensity (similar to those presented in Fig. 1) in the form of dependences of the relative effective radius $r_e = R_e/R_{e\infty}$ and the displacement of the centroid $\delta R_c = |\boldsymbol{R}_c| - |\boldsymbol{R}_{c\infty}|$ of the energy density distribution for the radiation subjected to filamentation along the air path on the type and tightness of initial focusing. Here, $R_{e\infty}$ and $\boldsymbol{R}_{c\infty}$ are, respectively, the effective radius and the radius vector of the centroid [5] of the profile of the collimated beam with the same initial power.

When calculating these parameters, we used an original software for analysing digital images. Each point in Fig. 2 was obtained by averaging r_e and δR_c values over 10–15 light energy density profiles, recorded at a chosen propagation distance, all other factors being equal. The displacement δR_c of the beam centroid was found by successive averaging: first we averaged the modulus of the radius vector of the centroid for a collimated beam, $|\boldsymbol{R}_{c\infty}|$, after which the difference in the corresponding values was averaged.

It can be seen that a decrease in the initial radius of the phase front curvature (decrease in $|f|$) leads on average to a more pronounced diffusion of the laser beam as a whole by the end of the path; note that, in view of the aforementioned factors, this diffusion is much more pronounced for a focused beam than for a defocused one. The centroid $|\boldsymbol{R}_{c\infty}|$ behaves similarly with a change in $|f|$: the displacement δR_c increases when the geometric focus of the telescope approaches the beginning of the path.

In the regime of relatively soft focusing, the radiation is focused or defocused so that $|f| \approx L$. In the first case, we have a diffused transverse energy profile in comparison with such of a collimated beam ($r_e \approx 1.3$). In the second case, vice versa, a higher energy concentration ($r_e \approx 0.75$) is observed. Here, no peculiar differences in the final position of the centroid of the beam intensity distribution were observed at $f < 0$ and $f > 0$. This result clearly indicates that with the optical focusing system being tuned on a specific experimental path, one can control the number and mutual position of peaks of the beam energy density in the receiving plane. Moreover, having performed a corresponding beam defocusing, one can in princi-

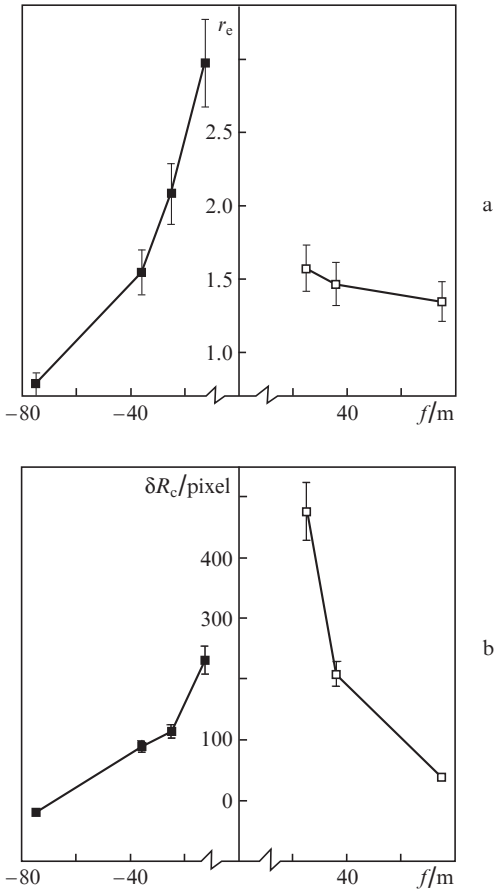

Figure 2. Dependences of the (a) effective normalised radius r_e and (b) the displacement of centroid δR_c of the transverse energy density distribution for a laser beam with P_0 = 93 GW after its propagation along an atmospheric path on the focal length f under different initial focusing conditions.

ple obtain a closer distribution of optical 'hot zones' in comparison with filamentation of collimated radiation with the same initial power.

2.2. Laboratory study of post-focal filamentation

Let us now consider the results of the experimental study of filament transmission through the laser beam focal plane.

Profiles of the laser beam energy at the output of the optical system and at a distance of 52 cm behind the mirror geometric focus ($f = 125$ cm) are shown in Figs 3a and 3b. It follows from these plots that aberrations of the initial beam shape lead to the formation of several filaments by the end of the optical path. Projections of five of them on the detecting screen can be seen well in Fig. 3b.

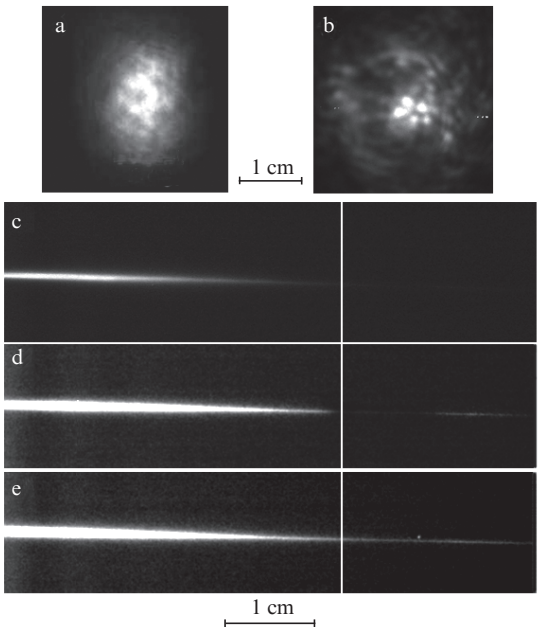

Figure 3. Transverse distributions of laser beam energy (a) at the beginning of the path and (b) at a distance of 52 cm and light filament images (side view) in the region of geometric focus (vertical solid line) at laser-pulse peak powers P_0 = (c) 170, (d) 270, and (e) 370 GW.

The plasma channel accompanying laser pulse filamentation stimulates fluorescence of molecular nitrogen in air, which manifests itself in blue light emitted from the filament. An example of detecting such a luminous region is shown in Figs 3c–e, which demonstrate regions of the beam focal waist near which a light filament arose at different laser pulse powers.

It can be seen that, at a power $P_0 = 170$ GW (Fig. 3c), which corresponds to a normalised pulse power $\eta \equiv P_0/P_c = 33$, the filament formation begins before the focal waist and ends almost at the geometric focus, i.e., at $z = f$. Behind the focus filamentation is absent. Provided that the spatial focusing sharpness is the same, a higher power laser pulse with $\eta = 53$ (Fig. 3d) first also undergoes filamentation before the linear focus, while behind the focus (at a distance of about 1 cm) the filament is extended by even more 0.5 cm. Finally, at even higher beam powers (Fig. 3e), a filament without breaks is observed throughout the entire focal waist.

It is convenient to introduce some generalised beam parameters for further analysis. Using these parameters, one can write a quantitative condition for laser beam self-focusing behind the focus of the optical system based on experimental data or rigorous numerical calculations. We will use the following generalised parameters: the 'force' of linear beam focusing, $\vartheta = L_d/f$, and the parameter of reduced radiation power, η ($L_d = k_0 R_0^2$ is the diffraction length for a beam of radius R_0, $k_0 = 2\pi/\lambda_0$, and λ_0 is the laser radiation wavelength).

To calculate the threshold power, depending on the laser beam focusing 'force', we performed numerical experiments with beams having different initial radii, powers, and focusing parameters. The propagation of focused USLPs in air was simulated by solving numerically the nonlinear Schrödinger equation (NSE) for the envelope of the light-wave electric field strength. This equation reliably describes all significant linear and nonlinear processes with participation of a laser pulse in a medium, at least at pulse durations not shorter than several optical periods (see, for example, reviews [1–5]). The model of optical nonlinearity of air included instantaneous and inertial components of the Kerr effect, as well as the change in the complex refractive index of the medium due to the photoionisation of gas molecules in air. The NSE linear part described the dispersion of the laser pulse group velocity and the beam diffraction.

Figure 4 shows a numerically calculated dependence of the threshold value ϑ_{th} of the dimensionless beam focusing parameter on the normalised initial (peak) laser pulse power η for the case where the light filament may expand beyond the linear beam focus. Here, we also presented our experimental data; the results of [16]; and the threshold for filament transmission through the geometric focus, calculated using the dependence [21]

$$\vartheta_{th} = \alpha\sqrt{\eta - 1}. \qquad (1)$$

The fitting coefficient α in (1) is, strictly speaking, a function of the initial beam power and the focusing parameter; it can be calculated based on the exact solution of the problem of USLP propagation in a medium. In our case it was chosen to approximate most exactly the numerical data: $\alpha = 7$.

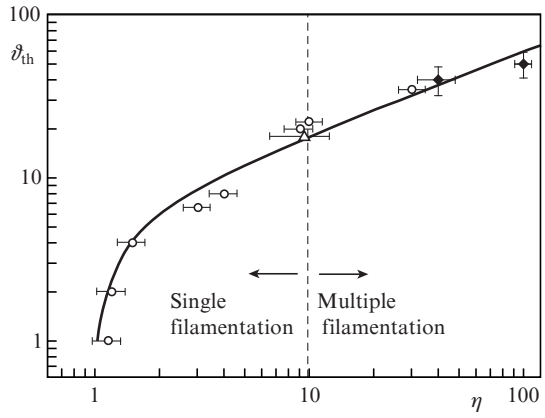

Figure 4. Dependence of the threshold focusing parameter at post-focal beam filamentation on the normalised power: (circles) results of numerical calculation, (diamonds) our experimental data, and (triangle) data of [16]; the solid curve is the result of calculation based on formula (1).

The results in Fig. 4 should be understood as follows: if at a fixed pulse power η the focusing parameter is below the threshold [i.e., $\vartheta < \vartheta_{th}(\eta)$], one would expect diffractionless beam propagation behind the focus, similar to its filamentation. In the opposite case [$\vartheta > \vartheta_{th}(\eta)$], the initial beam focusing will be too tight to implement expansion of filamentation behind the focal waist, and the filament will stop in the vicinity of the beam geometric focus.

The spread of values for the theoretical points is indicative of some arbitrariness in determining the threshold for filament transmission through the geometric focus: it was difficult to exactly determine the plasma electron density because of its sharp power-law dependence on the light-wave intensity.

The point in Fig. 4 that presents the experimental results of [16] was obtained by recalculating the data on the threshold power of 'refocusing' the initially focused (f = 1.5 m) beam with a radius of 2 mm, measured by us at a pulse energy in the range of 7.2–15 mJ.

In our experiments a similar threshold for transmission through the focal waist was established at the pulse power $P_0 \approx 200$ GW. Since the initial beam intensity profile significantly differed from Gaussian (Fig. 3a), the focusing parameter ϑ was recalculated with allowance for the real measured free diffraction length L_d, which turned out to be ~50 m (with a small error).

It is noteworthy that the range of laser powers in Fig. 4 corresponds to both single and multiple filamentation regimes. These regions are approximately separated by a vertical dashed line. At the same time, threshold relation (1) was derived within the model of single filament formation. Nevertheless, the points corresponding to numerical calculation and the experimental data obtained under the multiple filamentation conditions fit well the approximation curve for the single filamentation regime.

In the range of ϑ values corresponding to weak beam focusing ($\vartheta \sim 1$), the discrepancy between the results of calculation based on formula (1) and the numerical solution to NSE becomes more pronounced. An evident reason is that, for a weakly focused beam, the filamentation region expands to the linear focus. Therefore, the nonlinear loss of radiation on the formation of a plasma channel during photoionisation of air molecules increases as well. This leads to an additional beam divergence, and a higher power is required to compensate for the loss and implement filamentation behind the focal waist.

When predicting the propagation of a high-power wide-aperture quasi-parallel beam ($\eta \gg 1$, $\vartheta < 1$), the threshold expression (1) should be used with care. In the case where a laser beam has a multikilometre diffraction length and is spatially focused at even a larger distance, the filamentation region may even fail to reach the beam focal waist. On real atmospheric paths, along with increasing loss of light energy on the formation of plasma channels, destruction of filaments is facilitated by some other processes, for example, pulse chromatic dispersion and atmospheric turbulence. This situation must be considered separately; it is planned to do in our next studies.

3. Conclusions

We investigated the propagation of high-power femtosecond laser pulses with an initial highly inhomogeneous asymmetric transverse intensity profile on a 85-m atmospheric path in the self-focusing and filamentation regimes. It was shown that, using geometric focusing (or defocusing), one can control the spatial energy distribution for such laser beams in the receiving zone. It was established that, when focusing a laser beam, a decrease in the focal length causes a significant spreading of the beam image on the receiving screen in comparison with the collimated beam image. In this case, the regions with a high laser energy density, caused by beam filamentation, are not observed in the transverse beam cross section at the end of the path. Beam defocusing of the same 'force' also increases the transverse beam cross section area on the detector; however, it allows one to shift the beginning of the filamentation region at a larger distance along the path and expand (under certain conditions) this region to the receiving plane.

We performed a series of laboratory and numerical experiments to study the filamentation dynamics for a tightly focused femtosecond laser beam and determined the conditions under which a light filament formed before the geometric focus may survive after beam transmission through the focal plane. A semiempirical relation was obtained, which links the optical focusing 'force' and the initial laser pulse power (for $P_0 \leqslant 350$ GW) and sets a threshold for the post-focal beam filamentation. When this threshold is exceeded, the probability of filamentiation behind the lens focus increases, independent of the filamentation regime (single or multiple).

Acknowledgements. We are grateful to Yu.A. Mal'kov and D.I. Kulagin (Institute of Applied Physics, Russian Academy of Sciences) and D.V. Apeksimov and V.K. Oshlakov (Institute of Atmosphere Optics, Siberian Branch, Russian Academy of Sciences) for their help in preparing and carrying out experiments.

This work was supported by the programme 'Extreme Light Fields and Their Applications' of the Presidium of the Russian Academy of Sciences.

References

1. Berge L., Skupin S., Nuter R., Kasparian J., Wolf J.-P. *Rep. Prog. Phys*., **70**, 1633 (2007).
2. Couairon A., Myzyrowicz A. *Phys. Rep.*, **441**, 47 (2007).
3. Kandidov V.P., Shlenov S.A., Kosareva O.G. *Kvantovaya Elektron*., **39**, 205 (2009) [*Quantum Electron*., **39**, 205 (2009)].
4. Shen Y.R., Boyd R.W., Lukishova S.G. (Eds) *Self-focusing: Past and Present* (Berlin: Springer, 2009).
5. Geints Yu.E., Zemlyanov A.A., Kabanov A.M., Matvienko G.G., in: *Nelineinaya femtosekundnaya optika atmosfery* (Nonlinear Femtosecond Optics of Atmosphere) (Tomsk: Izd-vo Inst. Optiki Atmosfery SO RAN, 2010).
6. Fibich G., Sivan Y., Ehrlich Y., Louzon E., Fraenkel M., Eisenmann S., Katzir Y., Zigler A. *Opt. Express*, **14**, 4946 (2006).
7. Mechain G., Couairon A., Franco M., Prade B., Mysyrowicz A. *Phys. Rev. Lett*., **93**, 035003 (2004).
8. Kandidov V.P., Akozbek N., Scalora M., Kosareva O.G., Nyakk A.V., Luo Q., Hosseini S.A., Chin S.L. *Appl. Phys. B*, **80**, 267 (2005).
9. Roskey D.E., Kolesik M., Moloney J.V., Wright E.M. *Appl. Phys. B*, **86**, 249 (2007).
10. Hao Z.-Q., Zhang J., Xi T.-T., Yuan X.H., Zheng Z.Y., Lu X., Yu M.Y., Li Y.T., et al. *Opt. Express*, **15**, 16102 (2007).
11. Mechain G., Amico C.D., Andre Y.B., Tzortzakis S., Franco M., Prade B., Mysyrowicz A., Couairon A., Salmon E., Sauerbrey R. *Opt. Commun*., **247**, 171 (2005).
12. Fedorov V.Y., Shlenov S.A., Kandidov V.P. *Eur. Phys. J. D*, **50**, 185 (2008).
13. Liu W., Theberge F., Daigle J.-F., Simrad P.T., Kamali Y., Xu H.L., Chin S.L. *Appl. Phys. B*, **85**, 55 (2006).

14. Shlenov S.A., Markov A.I. *Kvantovaya Elektron*., **39**, 658 (2009) [*Quantum Electron*., **39**, 658 (2009)].
15. Kandidov V.P., Shlenov S.A., Silaeva E.P., Dergachev A.A. *Opt. Atmos. Okeana*, **23**, 873 (2010).
16. Talebpour A., Petit S., Chin S.L. *Opt. Commun*., **171**, 285 (1999).
17. Geints Yu.E., Zemlyanov A.A., Ionin A.A., Kudryashov S.I., Seleznev L.V., Sinitsyn D.V., Sunchugasheva E.S. *Zh. Eksp. Teor. Fiz*., **143**, 228 (2013).
18. Zemlyanov A.A., Bulygin A.D., Geints Yu.E. *Opt. Atmos. Okeana*, **24**, 839 (2011).
19. Geints Yu.E., Zemlyanov A.A., Kabanov A.M., Matvienko G.G., Stepanov A.N. *Opt. Atmos. Okeana*, **22**, 119 (2009).
20. Talanov V.I. *Pis'ma Zh. Eksp. Teor. Fiz*., **11**, 190 (1970).
21. Geints Yu.E., Zemlyanov A.A., Kabanov A.M., Matvienko G.G., Stepanov A.N. *Opt. Atmos. Okeana*, **25**, 745 (2012).